

Time-Dependent Analysis of the Decay $B^0 \rightarrow \rho^0 \rho^0$

The *BABAR* Collaboration

August 12, 2007

Abstract

We study the decay $B^0 \rightarrow \rho^0 \rho^0$ in a sample of about 427 million $\Upsilon(4S) \rightarrow B\bar{B}$ decays collected with the *BABAR* detector at the PEP-II asymmetric-energy e^+e^- collider at SLAC. We find the branching fraction $\mathcal{B} = (0.84 \pm 0.29 \pm 0.17) \times 10^{-6}$ and longitudinal polarization fraction of $f_L = 0.70 \pm 0.14 \pm 0.05$, where the first uncertainty is statistical, and the second is systematic. The evidence for the $B^0 \rightarrow \rho^0 \rho^0$ signal has 3.6σ significance. We investigate the proper-time dependence of the longitudinal component in the decay and measure the CP -violating coefficients $S_L^{00} = (0.5 \pm 0.9 \pm 0.2)$ and $C_L^{00} = (0.4 \pm 0.9 \pm 0.2)$, corresponding to the sine and cosine terms in the time evolution of asymmetry. We study the implication of these results for penguin contributions in $B \rightarrow \rho\rho$ decays and for the CKM unitarity angle α .

Contributed to the XXIIIrd International Symposium on Lepton and Photon Interactions at High Energies, 8/13 – 8/18/2007, Daegu, Korea

Stanford Linear Accelerator Center, Stanford University, Stanford, CA 94309

Work supported in part by US Department of Energy contract DE-AC02-76SF00515

The BABAR Collaboration,

B. Aubert, M. Bona, D. Boutigny, Y. Karyotakis, J. P. Lees, V. Poireau, X. Prudent, V. Tisserand,
A. Zghiche

*Laboratoire de Physique des Particules, IN2P3/CNRS et Université de Savoie, F-74941 Annecy-Le-Vieux,
France*

J. Garra Tico, E. Grauges

Universitat de Barcelona, Facultat de Física, Departament ECM, E-08028 Barcelona, Spain

L. Lopez, A. Palano, M. Pappagallo

Università di Bari, Dipartimento di Fisica and INFN, I-70126 Bari, Italy

G. Eigen, B. Stugu, L. Sun

University of Bergen, Institute of Physics, N-5007 Bergen, Norway

G. S. Abrams, M. Battaglia, D. N. Brown, J. Button-Shafer, R. N. Cahn, Y. Groysman, R. G. Jacobsen,
J. A. Kadyk, L. T. Kerth, Yu. G. Kolomensky, G. Kukartsev, D. Lopes Pegna, G. Lynch, L. M. Mir,
T. J. Orimoto, I. L. Osipenkov, M. T. Ronan,¹ K. Tackmann, T. Tanabe, W. A. Wenzel

Lawrence Berkeley National Laboratory and University of California, Berkeley, California 94720, USA

P. del Amo Sanchez, C. M. Hawkes, A. T. Watson

University of Birmingham, Birmingham, B15 2TT, United Kingdom

H. Koch, T. Schroeder

Ruhr Universität Bochum, Institut für Experimentalphysik 1, D-44780 Bochum, Germany

D. Walker

University of Bristol, Bristol BS8 1TL, United Kingdom

D. J. Asgeirsson, T. Cuhadar-Donszelmann, B. G. Fulsom, C. Hearty, T. S. Mattison, J. A. McKenna

University of British Columbia, Vancouver, British Columbia, Canada V6T 1Z1

M. Barrett, A. Khan, M. Saleem, L. Teodorescu

Brunel University, Uxbridge, Middlesex UB8 3PH, United Kingdom

V. E. Blinov, A. D. Bukin, V. P. Druzhinin, V. B. Golubev, A. P. Onuchin, S. I. Serednyakov,
Yu. I. Skovpen, E. P. Solodov, K. Yu. Todyshev

Budker Institute of Nuclear Physics, Novosibirsk 630090, Russia

M. Bondioli, S. Curry, I. Eschrich, D. Kirkby, A. J. Lankford, P. Lund, M. Mandelkern, E. C. Martin,
D. P. Stoker

University of California at Irvine, Irvine, California 92697, USA

S. Abachi, C. Buchanan

University of California at Los Angeles, Los Angeles, California 90024, USA

S. D. Foulkes, J. W. Gary, F. Liu, O. Long, B. C. Shen,¹ G. M. Vitug, L. Zhang

University of California at Riverside, Riverside, California 92521, USA

¹Deceased

H. P. Paar, S. Rahatlou, V. Sharma

University of California at San Diego, La Jolla, California 92093, USA

J. W. Berryhill, C. Campagnari, A. Cunha, B. Dahmes, T. M. Hong, D. Kovalskyi, J. D. Richman

University of California at Santa Barbara, Santa Barbara, California 93106, USA

T. W. Beck, A. M. Eisner, C. J. Flacco, C. A. Heusch, J. Kroseberg, W. S. Lockman, T. Schalk,
B. A. Schumm, A. Seiden, M. G. Wilson, L. O. Winstrom

University of California at Santa Cruz, Institute for Particle Physics, Santa Cruz, California 95064, USA

E. Chen, C. H. Cheng, F. Fang, D. G. Hitlin, I. Narsky, T. Piatenko, F. C. Porter

California Institute of Technology, Pasadena, California 91125, USA

R. Andreassen, G. Mancinelli, B. T. Meadows, K. Mishra, M. D. Sokoloff

University of Cincinnati, Cincinnati, Ohio 45221, USA

F. Blanc, P. C. Bloom, S. Chen, W. T. Ford, J. F. Hirschauer, A. Kreisel, M. Nagel, U. Nauenberg,
A. Olivas, J. G. Smith, K. A. Ulmer, S. R. Wagner, J. Zhang

University of Colorado, Boulder, Colorado 80309, USA

A. M. Gabareen, A. Soffer,² W. H. Toki, R. J. Wilson, F. Winklmeier

Colorado State University, Fort Collins, Colorado 80523, USA

D. D. Altenburg, E. Feltresi, A. Hauke, H. Jasper, J. Merkel, A. Petzold, B. Spaan, K. Wacker

Universität Dortmund, Institut für Physik, D-44221 Dortmund, Germany

V. Klose, M. J. Kobel, H. M. Lacker, W. F. Mader, R. Nogowski, J. Schubert, K. R. Schubert, R. Schwierz,
J. E. Sundermann, A. Volk

Technische Universität Dresden, Institut für Kern- und Teilchenphysik, D-01062 Dresden, Germany

D. Bernard, G. R. Bonneaud, E. Latour, V. Lombardo, Ch. Thiebaux, M. Verderi

Laboratoire Leprince-Ringuet, CNRS/IN2P3, Ecole Polytechnique, F-91128 Palaiseau, France

P. J. Clark, W. Gradl, F. Muheim, S. Playfer, A. I. Robertson, J. E. Watson, Y. Xie

University of Edinburgh, Edinburgh EH9 3JZ, United Kingdom

M. Andreotti, D. Bettoni, C. Bozzi, R. Calabrese, A. Cecchi, G. Cibinetto, P. Franchini, E. Luppi,
M. Negrini, A. Petrella, L. Piemontese, E. Prencipe, V. Santoro

Università di Ferrara, Dipartimento di Fisica and INFN, I-44100 Ferrara, Italy

F. Anulli, R. Baldini-Ferrolì, A. Calcaterra, R. de Sangro, G. Finocchiaro, S. Pacetti, P. Patteri,
I. M. Peruzzi,³ M. Piccolo, M. Rama, A. Zallo

Laboratori Nazionali di Frascati dell'INFN, I-00044 Frascati, Italy

A. Buzzo, R. Contri, M. Lo Vetere, M. M. Macri, M. R. Monge, S. Passaggio, C. Patrignani, E. Robutti,
A. Santroni, S. Tosi

Università di Genova, Dipartimento di Fisica and INFN, I-16146 Genova, Italy

²Now at Tel Aviv University, Tel Aviv, 69978, Israel

³Also with Università di Perugia, Dipartimento di Fisica, Perugia, Italy

K. S. Chaisanguanthum, M. Morii, J. Wu
Harvard University, Cambridge, Massachusetts 02138, USA

R. S. Dubitzky, J. Marks, S. Schenk, U. Uwer
Universität Heidelberg, Physikalisches Institut, Philosophenweg 12, D-69120 Heidelberg, Germany

D. J. Bard, P. D. Dauncey, R. L. Flack, J. A. Nash, W. Panduro Vazquez, M. Tibbetts
Imperial College London, London, SW7 2AZ, United Kingdom

P. K. Behera, X. Chai, M. J. Charles, U. Mallik
University of Iowa, Iowa City, Iowa 52242, USA

J. Cochran, H. B. Crawley, L. Dong, V. Eyges, W. T. Meyer, S. Prell, E. I. Rosenberg, A. E. Rubin
Iowa State University, Ames, Iowa 50011-3160, USA

Y. Y. Gao, A. V. Griksan, Z. J. Guo, C. K. Lae
Johns Hopkins University, Baltimore, Maryland 21218, USA

A. G. Denig, M. Fritsch, G. Schott
Universität Karlsruhe, Institut für Experimentelle Kernphysik, D-76021 Karlsruhe, Germany

N. Arnaud, J. Béquilleux, A. D’Orazio, M. Davier, G. Grosdidier, A. Höcker, V. Lepeltier, F. Le Diberder,
A. M. Lutz, S. Pruvot, S. Rodier, P. Roudeau, M. H. Schune, J. Serrano, V. Sordini, A. Stocchi, L. Wang,
W. F. Wang, G. Wormser

*Laboratoire de l’Accélérateur Linéaire, IN2P3/CNRS et Université Paris-Sud 11, Centre Scientifique
d’Orsay, B. P. 34, F-91898 ORSAY Cedex, France*

D. J. Lange, D. M. Wright
Lawrence Livermore National Laboratory, Livermore, California 94550, USA

I. Bingham, J. P. Burke, C. A. Chavez, J. R. Fry, E. Gabathuler, R. Gamet, D. E. Hutchcroft, D. J. Payne,
K. C. Schofield, C. Touramanis

University of Liverpool, Liverpool L69 7ZE, United Kingdom

A. J. Bevan, K. A. George, F. Di Lodovico, R. Sacco, M. Sigamani
Queen Mary, University of London, E1 4NS, United Kingdom

G. Cowan, H. U. Flaecher, D. A. Hopkins, S. Paramesvaran, F. Salvatore, A. C. Wren
*University of London, Royal Holloway and Bedford New College, Egham, Surrey TW20 0EX, United
Kingdom*

D. N. Brown, C. L. Davis
University of Louisville, Louisville, Kentucky 40292, USA

J. Allison, N. R. Barlow, R. J. Barlow, Y. M. Chia, C. L. Edgar, G. D. Lafferty, T. J. West, J. I. Yi
University of Manchester, Manchester M13 9PL, United Kingdom

J. Anderson, C. Chen, A. Jawahery, D. A. Roberts, G. Simi, J. M. Tuggle
University of Maryland, College Park, Maryland 20742, USA

G. Blaylock, C. Dallapiccola, S. S. Hertzbach, X. Li, T. B. Moore, E. Salvati, S. Saremi
University of Massachusetts, Amherst, Massachusetts 01003, USA

R. Cowan, D. Dujmic, P. H. Fisher, K. Koenke, G. Sciolla, M. Spitznagel, F. Taylor, R. K. Yamamoto,
M. Zhao, Y. Zheng
*Massachusetts Institute of Technology, Laboratory for Nuclear Science, Cambridge, Massachusetts 02139,
USA*

S. E. Mclachlin,¹ P. M. Patel, S. H. Robertson
McGill University, Montréal, Québec, Canada H3A 2T8

A. Lazzaro, F. Palombo
Università di Milano, Dipartimento di Fisica and INFN, I-20133 Milano, Italy

J. M. Bauer, L. Cremaldi, V. Eschenburg, R. Godang, R. Kroeger, D. A. Sanders, D. J. Summers,
H. W. Zhao
University of Mississippi, University, Mississippi 38677, USA

S. Brunet, D. Côté, M. Simard, P. Taras, F. B. Viaud
Université de Montréal, Physique des Particules, Montréal, Québec, Canada H3C 3J7

H. Nicholson
Mount Holyoke College, South Hadley, Massachusetts 01075, USA

G. De Nardo, F. Fabozzi,⁴ L. Lista, D. Monorchio, C. Sciacca
Università di Napoli Federico II, Dipartimento di Scienze Fisiche and INFN, I-80126, Napoli, Italy

M. A. Baak, G. Raven, H. L. Snoek
*NIKHEF, National Institute for Nuclear Physics and High Energy Physics, NL-1009 DB Amsterdam, The
Netherlands*

C. P. Jessop, K. J. Knoepfel, J. M. LoSecco
University of Notre Dame, Notre Dame, Indiana 46556, USA

G. Benelli, L. A. Corwin, K. Honscheid, H. Kagan, R. Kass, J. P. Morris, A. M. Rahimi,
J. J. Regensburger, S. J. Sekula, Q. K. Wong
Ohio State University, Columbus, Ohio 43210, USA

N. L. Blount, J. Brau, R. Frey, O. Igonkina, J. A. Kolb, M. Lu, R. Rahmat, N. B. Sinev, D. Strom,
J. Strube, E. Torrence
University of Oregon, Eugene, Oregon 97403, USA

N. Gagliardi, A. Gaz, M. Margoni, M. Morandin, A. Pompili, M. Posocco, M. Rotondo, F. Simonetto,
R. Stroili, C. Voci
Università di Padova, Dipartimento di Fisica and INFN, I-35131 Padova, Italy

E. Ben-Haim, H. Briand, G. Calderini, J. Chauveau, P. David, L. Del Buono, Ch. de la Vaissière,
O. Hamon, Ph. Leruste, J. Malclès, J. Ocariz, A. Perez, J. Prendki
*Laboratoire de Physique Nucléaire et de Hautes Energies, IN2P3/CNRS, Université Pierre et Marie
Curie-Paris6, Université Denis Diderot-Paris7, F-75252 Paris, France*

⁴Also with Università della Basilicata, Potenza, Italy

L. Gladney

University of Pennsylvania, Philadelphia, Pennsylvania 19104, USA

M. Biasini, R. Covarelli, E. Manoni

Università di Perugia, Dipartimento di Fisica and INFN, I-06100 Perugia, Italy

C. Angelini, G. Batignani, S. Bettarini, M. Carpinelli,⁵ R. Cenci, A. Cervelli, F. Forti, M. A. Giorgi,
A. Lusiani, G. Marchiori, M. A. Mazur, M. Morganti, N. Neri, E. Paoloni, G. Rizzo, J. J. Walsh

Università di Pisa, Dipartimento di Fisica, Scuola Normale Superiore and INFN, I-56127 Pisa, Italy

J. Biesiada, P. Elmer, Y. P. Lau, C. Lu, J. Olsen, A. J. S. Smith, A. V. Telnov

Princeton University, Princeton, New Jersey 08544, USA

E. Baracchini, F. Bellini, G. Cavoto, D. del Re, E. Di Marco, R. Faccini, F. Ferrarotto, F. Ferroni,
M. Gaspero, P. D. Jackson, L. Li Gioi, M. A. Mazzoni, S. Morganti, G. Piredda, F. Polci, F. Renga,
C. Voena

Università di Roma La Sapienza, Dipartimento di Fisica and INFN, I-00185 Roma, Italy

M. Ebert, T. Hartmann, H. Schröder, R. Waldi

Universität Rostock, D-18051 Rostock, Germany

T. Adye, G. Castelli, B. Franek, E. O. Olaiya, W. Roethel, F. F. Wilson

Rutherford Appleton Laboratory, Chilton, Didcot, Oxon, OX11 0QX, United Kingdom

S. Emery, M. Escalier, A. Gaidot, S. F. Ganzhur, G. Hamel de Monchenault, W. Kozanecki, G. Vasseur,
Ch. Yèche, M. Zito

DSM/Daphnia, CEA/Saclay, F-91191 Gif-sur-Yvette, France

X. R. Chen, H. Liu, W. Park, M. V. Purohit, R. M. White, J. R. Wilson,

University of South Carolina, Columbia, South Carolina 29208, USA

M. T. Allen, D. Aston, R. Bartoldus, P. Bechtle, R. Claus, J. P. Coleman, M. R. Convery, J. C. Dingfelder,
J. Dorfan, G. P. Dubois-Felsmann, W. Dunwoodie, R. C. Field, T. Glanzman, S. J. Gowdy, M. T. Graham,
P. Grenier, C. Hast, W. R. Innes, J. Kaminski, M. H. Kelsey, H. Kim, P. Kim, M. L. Kocian,
D. W. G. S. Leith, S. Li, S. Luitz, V. Luth, H. L. Lynch, D. B. MacFarlane, H. Marsiske, R. Messner,
D. R. Muller, S. Nelson, C. P. O'Grady, I. Ofte, A. Perazzo, M. Perl, T. Pulliam, B. N. Ratcliff,
A. Roodman, A. A. Salnikov, R. H. Schindler, J. Schwiening, A. Snyder, D. Su, S. Sun, M. K. Sullivan,
K. Suzuki, S. K. Swain, J. M. Thompson, J. Va'vra, A. P. Wagner, M. Weaver, W. J. Wisniewski,
M. Wittgen, D. H. Wright, A. K. Yarritu, K. Yi, C. C. Young, V. Ziegler

Stanford Linear Accelerator Center, Stanford, California 94309, USA

P. R. Burchat, A. J. Edwards, S. A. Majewski, T. S. Miyashita, B. A. Petersen, L. Wilden

Stanford University, Stanford, California 94305-4060, USA

S. Ahmed, M. S. Alam, R. Bula, J. A. Ernst, V. Jain, B. Pan, M. A. Saeed, F. R. Wappler, S. B. Zain

State University of New York, Albany, New York 12222, USA

M. Krishnamurthy, S. M. Spanier, B. J. Wogslund

University of Tennessee, Knoxville, Tennessee 37996, USA

⁵Also with Università di Sassari, Sassari, Italy

R. Eckmann, J. L. Ritchie, A. M. Ruland, C. J. Schilling, R. F. Schwitters
University of Texas at Austin, Austin, Texas 78712, USA

J. M. Izen, X. C. Lou, S. Ye
University of Texas at Dallas, Richardson, Texas 75083, USA

F. Bianchi, F. Gallo, D. Gamba, M. Pelliccioni
Università di Torino, Dipartimento di Fisica Sperimentale and INFN, I-10125 Torino, Italy

M. Bomben, L. Bosisio, C. Cartaro, F. Cossutti, G. Della Ricca, L. Lanceri, L. Vitale
Università di Trieste, Dipartimento di Fisica and INFN, I-34127 Trieste, Italy

V. Azzolini, N. Lopez-March, F. Martinez-Vidal,⁶ D. A. Milanes, A. Oyanguren
IFIC, Universitat de Valencia-CSIC, E-46071 Valencia, Spain

J. Albert, Sw. Banerjee, B. Bhuyan, K. Hamano, R. Kowalewski, I. M. Nugent, J. M. Roney, R. J. Sobie
University of Victoria, Victoria, British Columbia, Canada V8W 3P6

P. F. Harrison, J. Ilic, T. E. Latham, G. B. Mohanty
Department of Physics, University of Warwick, Coventry CV4 7AL, United Kingdom

H. R. Band, X. Chen, S. Dasu, K. T. Flood, J. J. Hollar, P. E. Kutter, Y. Pan, M. Pierini, R. Prepost,
S. L. Wu
University of Wisconsin, Madison, Wisconsin 53706, USA

H. Neal
Yale University, New Haven, Connecticut 06511, USA

⁶Also with Universitat de Barcelona, Facultat de Fisica, Departament ECM, E-08028 Barcelona, Spain

1 INTRODUCTION

Measurements of CP -violating asymmetries in the $B^0\bar{B}^0$ system test the flavor structure of the standard model by over-constraining the Cabibbo-Kobayashi-Maskawa (CKM) quark-mixing matrix [1]. The time-dependent CP asymmetry in the decays of B^0 or \bar{B}^0 mesons to a CP eigenstate dominated by the tree-level amplitude $b \rightarrow u\bar{u}d$ measures $\sin 2\alpha_{\text{eff}}$, where α_{eff} differs from the CKM unitarity triangle angle $\alpha \equiv \arg[-V_{td}V_{tb}^*/V_{ud}V_{ub}^*]$ by a quantity $\Delta\alpha$ accounting for the contributions from loop (penguin) amplitudes. The value of $\Delta\alpha$ can be extracted from an analysis of the branching fractions of the B decays into the full set of isospin-related channels [2].

Branching fractions and time-dependent CP asymmetries in $B \rightarrow \pi\pi$, $\rho\pi$, and $\rho\rho$ have already provided information on α . Since the tree contribution to the $B^0 \rightarrow \rho^0\rho^0$ [3] decay is color-suppressed, the decay rate is sensitive to the penguin amplitude. The $B^0 \rightarrow \rho^0\rho^0$ decay has a much smaller branching fraction than $B^0 \rightarrow \rho^+\rho^-$ and $B^+ \rightarrow \rho^+\rho^0$ channels [4, 5, 6, 7, 8], which leads to a more stringent limit on $\Delta\alpha$ from isospin analysis [2, 7, 12] than is possible in $\pi\pi$ system. This makes the $\rho\rho$ system particularly effective for measuring α .

The error due to the penguin contribution becomes the dominant uncertainty in the measurement of α using $B \rightarrow \rho\rho$ decays. However, in contrast to $B \rightarrow \pi^0\pi^0$ decays, the four-track final state makes a time-dependent analysis of $B^0 \rightarrow \rho^0\rho^0$ decays feasible. It allows us to measure the CP parameters S_L^{00} and C_L^{00} directly, analogous to S_L^{+-} and C_L^{+-} , resolving ambiguities inherent to isospin triangle orientations. The C^{00} coefficient is associated with the difference in decay amplitudes for $B \rightarrow \rho^0\rho^0$ and $\bar{B} \rightarrow \rho^0\rho^0$, while the S^{00} coefficient involves interference between the $B^0 - \bar{B}^0$ mixing and decay amplitudes.

In $B \rightarrow \rho\rho$ decays the final state is a superposition of CP -odd and CP -even states. An isospin-triangle relation [2] holds for each of the three helicity amplitudes, which can be separated through an angular analysis. The helicity angles θ_1 and θ_2 are defined as the angles between the direction of π^+ and the direction of the B in the rest system of each of the ρ^0 candidates. The resulting angular distribution is given by

$$d^2\Gamma/(\Gamma d\cos\theta_1 d\cos\theta_2) = \frac{9}{4} \left\{ \frac{1}{4}(1 - f_L) \sin^2\theta_1 \sin^2\theta_2 + f_L \cos^2\theta_1 \cos^2\theta_2 \right\}, \quad (1)$$

where $f_L = |A_0|^2/(\sum|A_\lambda|^2)$ is the longitudinal polarization fraction and $A_{\lambda=-1,0,+1}$ are the helicity amplitudes. The fraction of longitudinal polarization is *a priori* unknown. Polarization was expected to be predominantly longitudinal [9]. However, significant departure from this expectation was found in penguin-dominated B -decay modes [10] and polarization and CP -asymmetry measurements in the $B^0 \rightarrow \rho^0\rho^0$ decay may help in resolving this puzzle [11].

In this paper, we update our previous measurement of the branching fraction and longitudinal polarization fraction in $B^0 \rightarrow \rho^0\rho^0$ decays [4], and present the first study of the time-dependent CP asymmetry \mathcal{A}_{CP} in this mode. We determine the coefficients C_L^{00} and S_L^{00} of the asymmetry for the longitudinal component, which is given by

$$\mathcal{A}_{CP}(\Delta t) = -C_L^{00} \cos \Delta m \Delta t + S_L^{00} \sin \Delta m \Delta t \quad (2)$$

These coefficients, together with improved measurements of the branching fraction and longitudinal polarization, allow a complete isospin analysis and improved constraints on the penguin contribution to $B \rightarrow \rho\rho$ decays. Changes with respect to our previous analysis [4] include increased datasample, improved track-selection techniques, and inclusion of the B -decay time information.

2 DETECTOR AND DATASET

These results are based on data collected with the *BABAR* detector [13] at the PEP-II asymmetric-energy e^+e^- collider [14]. A sample of 427 ± 5 million $B\bar{B}$ pairs was recorded at the $\Upsilon(4S)$ resonance with the center-of-mass (c.m.) energy $\sqrt{s} = 10.58$ GeV. Charged-particle momenta and trajectories are measured in a tracking system consisting of a five-layer double-sided silicon vertex tracker and a 40-layer drift chamber, both within a 1.5-T solenoidal magnetic field. Charged-particle identification is provided by measurements of the energy loss in the tracking devices and by a ring-imaging Cherenkov detector.

3 ANALYSIS METHOD

We select $B \rightarrow M_1 M_2 \rightarrow (\pi^+ \pi^-)(\pi^+ \pi^-)$ candidates, with $M_{1,2}$ standing for a ρ^0 or f_0 candidate, from neutral combinations of four charged tracks that are consistent with originating from a single vertex near the e^+e^- interaction point. We veto tracks that are identified as kaons or electrons. The identification of signal B candidates is based on several kinematic variables. The beam-energy-substituted mass, $m_{\text{ES}} = [(s/2 + \mathbf{p}_i \cdot \mathbf{p}_B)^2 / E_i^2 - \mathbf{p}_B^2]^{1/2}$, where the initial e^+e^- four-momentum (E_i, \mathbf{p}_i) and the B momentum \mathbf{p}_B are defined in the laboratory frame, is centered near the B mass with a resolution of 2.6 MeV/ c^2 for signal candidates. The difference $\Delta E = E_B^{\text{cm}} - \sqrt{s}/2$ between the reconstructed B energy in the c.m. frame and its known value $\sqrt{s}/2$ has a maximum near zero with a resolution of 20 MeV for signal events. Four other kinematic variables describe two possible $\pi^+ \pi^-$ pairs: the invariant masses m_1, m_2 and the helicity angles θ_1, θ_2 .

The selection requirements for signal candidates are the following: $5.245 < m_{\text{ES}} < 5.290$ GeV/ c^2 , $|\Delta E| < 85$ MeV, $550 < m_{1,2} < 1050$ MeV/ c^2 , and $|\cos \theta_{1,2}| < 0.98$. The last requirement removes a region corresponding to low-momentum pions with low and uncertain reconstruction efficiency. In addition, we veto the copious decays $B^0 \rightarrow D^{(*)-} \pi^+ \rightarrow (h^+ \pi^- \pi^-) \pi^+$, where h^+ refers to a pion or kaon, by requiring the invariant mass of the three-particle combination to differ from the D -meson mass by more than 13.2 MeV/ c^2 , or 40 MeV/ c^2 if one of the particles is consistent with a kaon hypothesis.

We reject the dominant $e^+e^- \rightarrow q\bar{q}$ ($q = u, d, s, c$) (continuum) background by requiring $|\cos \theta_T| < 0.8$, where θ_T is the angle between the B -candidate thrust axis and that of the remaining tracks and neutral clusters in the event, calculated in the c.m. frame. We further suppress continuum background using a neural network-based discriminant \mathcal{E} , which combines eight topological variables calculated in the c.m. frame. In addition to $\cos \theta_T$, they are the polar angles of the B momentum vector and the B -candidate thrust axis with respect to the beam axis, the value of the event thrust, two Legendre moments L_0 and L_2 of the energy flow around the B -candidate thrust axis [15] computed separately for neutral and charged particles, and the sum of the transverse momenta of all particles in the rest of the event, calculated with respect to the B direction.

We use multivariate B -flavor-tagging algorithms trained to identify primary leptons, kaons, soft pions, and high-momentum charged particles from the other B , called B_{tag} [17]. The effective tagging efficiency, which takes into account the efficiency to find the tag and the mistag probability, is $(31.1 \pm 0.3)\%$, as determined on a sample of fully reconstructed open-charm decays. We use both tagged and untagged events in our sample. Additional background discrimination power arises from the difference between the tagging efficiencies for signal and background in seven tagging categories ($c_{\text{tag}} = 1.7$). We determine the proper time difference Δt between the signal B and B_{tag} from the spatial separation between their decay vertices. The B_{tag} vertex is reconstructed

from the remaining charged tracks in the event and its uncertainty dominates the Δt resolution $\sigma_{\Delta t}$. The average proper time resolution is $\langle\sigma_{\Delta t}\rangle \approx 0.7$ ps. Only events that satisfy $|\Delta t| < 15$ ps and $\sigma_{\Delta t} < 2.5$ ps are retained.

After application of all selection criteria, $N_{\text{cand}} = 65637$ events form the sample for the maximum likelihood fit. On average, each selected event has 1.05 signal candidates, while in Monte Carlo [16] samples of longitudinally and transversely polarized $B^0 \rightarrow \rho^0 \rho^0$ decays we find 1.15 and 1.03 candidates, respectively. When more than one candidate is present in the same event, the candidate having the best χ^2 consistency with a single four-pion vertex is selected. Simulation shows that 18% of longitudinally and 4% of transversely polarized $B^0 \rightarrow \rho^0 \rho^0$ events are misreconstructed with one or more tracks not originating from the $B^0 \rightarrow \rho^0 \rho^0$ decay. These are mostly due to combinatorial background from low-momentum tracks from the other B meson in the event. Such events still carry the characteristic topology of $B^0 \rightarrow \rho^0 \rho^0$ events; they are modeled separately from the perfectly reconstructed events and included into the probability density functions.

4 MAXIMUM LIKELIHOOD FIT

We use an unbinned extended maximum likelihood fit to extract the $B^0 \rightarrow \rho^0 \rho^0$ event yield and fraction of longitudinal polarization f_L . We also fit for the event yields of $B^0 \rightarrow \rho^0 f_0$ and $B^0 \rightarrow f_0 f_0$ decays, as well as yields in several background categories. The likelihood function is

$$\mathcal{L} = \exp\left(-\sum_k n_k\right) \prod_{i=1}^{N_{\text{cand}}} \left(\sum_j n_j \mathcal{P}_j(\vec{x}_i)\right), \quad (3)$$

where n_j is the unconstrained (except if noted otherwise) number of events for each event type j ($B^0 \rightarrow \rho^0 \rho^0$, $B^0 \rightarrow \rho^0 f_0(980)$, $B^0 \rightarrow f_0(980)f_0(980)$, several background components from exclusive and inclusive B decays, and continuum), and $\mathcal{P}_j(\vec{x}_i)$ is the probability density function (PDF) of the variables $\vec{x}_i = \{m_{\text{ES}}, \Delta E, \mathcal{E}, m_1, m_2, \cos \theta_1, \cos \theta_2, c_{\text{tag}}, \Delta t, \sigma_{\Delta t}\}_i$ for the i th event.

Since the statistical correlations among most variables are found to be small, we take each \mathcal{P}_j as the product of the PDFs for the separate variables. In a number of special cases, for the mass-helicity PDF of continuum backgrounds, or for the mass and helicity PDFs of the B backgrounds, we use 2- or 4-dimensional PDFs to properly describe the kinematic correlation between the observables.

We use double-Gaussian functions to parameterize the m_{ES} PDFs for fully-reconstructed signal events, double-Gaussian functions for ΔE and relativistic Breit-Wigner functions for the resonance masses of ρ^0 and $f_0(980)$ [18]. The angular distribution at production for $B^0 \rightarrow \rho^0 \rho^0$, $B^0 \rightarrow \rho^0 f_0$, and $B^0 \rightarrow f_0 f_0$ modes (expressed as a function of the longitudinal polarization in Eq. (1) for $B^0 \rightarrow \rho^0 \rho^0$) is multiplied by a detector acceptance function $\mathcal{G}(\cos \theta_1, \cos \theta_2)$, determined from Monte Carlo. The distributions of misreconstructed signal events are parameterized with empirical shapes in a way similar to that used for B background discussed below. The neural network discriminant \mathcal{E} is described by two (continuum) or three (B -decay events) asymmetric Gaussian functions with different parameters for signal and background distributions.

The PDFs for inclusive B decay modes are generally modeled with empirical analytical distributions. Several variables have distributions similar or identical to those for signal, such as m_{ES} when all four tracks come from the same B , or $\pi^+ \pi^-$ invariant mass $m_{1,2}$ when both tracks come from a ρ^0 meson. Also for some of the modes the two $\pi^+ \pi^-$ pairs can have different mass and helicity distributions, *e.g.* when only one of the two combinations comes from a genuine ρ^0 or f_0

meson, or when one of the two pairs contains a high-momentum pion (as in $B \rightarrow a_1\pi$). In such cases, we use a four-dimensional mass-helicity PDF.

The proper-time distribution for signal and background B decays

$$f(\Delta t, Q) \sim \frac{e^{-|\Delta t|/\tau}}{4\tau} \times \left\{ 1 - Q\Delta w + Q\mu(1 - 2\omega) + [Q(1 - 2w) + \mu(1 - Q\Delta\omega)] \mathcal{A}_{CP}(\Delta t) \right\} \quad (4)$$

is convolved with a resolution function, modeled as a superposition of three Gaussian distributions with the means and widths scaled by the per-event error on Δt . Here Q is the flavor of B_{tag} , w is the average mistag probability, and Δw and μ parameters describe the difference in mistag probability and the tagging efficiency asymmetry between B^0 and \bar{B}^0 mesons. The time distribution of continuum background is assumed to have zero lifetime.

The signal and B -background PDF parameters are extracted from simulation. The Monte Carlo parameters for m_{ES} , ΔE , and \mathcal{E} PDFs are adjusted by comparing data and simulation in control channels with similar kinematics and topology, such as $B^0 \rightarrow D^-\pi^+$ with $D^- \rightarrow K^+\pi^-\pi^-$. The continuum background PDF shapes are extracted from off-resonance data or on-resonance sideband data, with parameters of the most discriminating PDFs (m_{ES} , ΔE , \mathcal{E}) left free in the final fit. The discrete B -flavor tagging PDFs and parameters of the proper time distributions for signal modes are obtained in dedicated fits to events with identified exclusive B decays [17]. The tagging PDFs for inclusive B backgrounds are determined by Monte Carlo and their systematic uncertainties are studied in data.

Backgrounds from “charmless” $b \rightarrow u$ transitions, in particular events containing ρ , f_0 , or K^* mesons, have kinematic distributions similar to those of signal events. We study the contributions of the dominant decay modes in high-statistics exclusive Monte Carlo samples. We also develop two complementary strategies to model these backgrounds in the likelihood fit.

In the first approach, we single out contributions from the following dominant modes: $B^0 \rightarrow a_1^\pm\pi^\mp$, $B^0 \rightarrow \rho^0 K^{*0}$, $B^0 \rightarrow f_0 K^{*0}$, $B^+ \rightarrow \rho^+\rho^0$, $B^+ \rightarrow a_1^0\pi^+$, $B \rightarrow \eta'K$, and $B^+ \rightarrow \rho^0\pi^+$. The contribution of the $B^0 \rightarrow a_1^\pm\pi^\mp$ decays includes both events where all four tracks are correctly associated to the B candidate, and events where at least one of the tracks is picked from the other B meson (so-called $B^0 \rightarrow a_1^\pm\pi^\mp$ “self-crossfeed” events). The event yield of the $B^0 \rightarrow a_1^\pm\pi^\mp$ decays is allowed to vary in the fit, while the yields of other six charmless modes listed above are fixed to the expected values [19, 20, 21]. The events from open charm $b \rightarrow c$ transitions are parameterized as a separate background component, with its yield allowed to vary in the data fit.

In the second strategy, we split the B background into three distinct categories: $B^0 \rightarrow a_1^\pm\pi^\mp$ decays where all four tracks are correctly associated with the B candidate, an appropriately weighted combination of dominant charmless decays, and the rest of the generic $b \rightarrow u$, $b \rightarrow c$, $b \rightarrow s$, and $b \rightarrow d$ transitions. For the charmless event category, we combine the following modes: $B^0 \rightarrow a_1^\pm\pi^\mp$ self-crossfeed events, $B^0 \rightarrow \rho^0 K^{*0}$, $B^0 \rightarrow f_0 K^{*0}$, $B^0 \rightarrow \rho^+\rho^-$, $B^0 \rightarrow \rho^\pm\pi^\mp$, $B^+ \rightarrow \rho^+\rho^0$, $B^+ \rightarrow a_1^0\pi^+$, $B^+ \rightarrow a_1^+ f_0$, $B \rightarrow \eta'K$, and $B^+ \rightarrow \rho^0\pi^+$. Kinematic distributions in these events, especially events in which at least one charged particle was not correctly associated to the B candidate, are similar to each other, and also to other, poorly measured charmless decays. This allows us to vary the overall event yield for this category of events, after fixing the relative weights of each mode to the expected values [19, 20, 21]. For yet-unmeasured $\mathcal{B}(B^+ \rightarrow a_1^+ f_0)$, we assume a conservative value of $(1 \pm 1) \times 10^{-5}$; this branching ratio corresponds to the expectation of 10 ± 10 events in the selected data sample. Event yields associated with $B^0 \rightarrow a_1^\pm\pi^\mp$ component and the generic B decays are allowed to vary in the maximum likelihood fit.

We find that both strategies for describing B decay backgrounds presented above adequately

describe the data, and are in excellent agreement on the yields, polarization, and CP parameters of $B^0 \rightarrow \rho^0 \rho^0$ decays. Statistical correlation between the two models is high (93% for the yields and f_L , 85% for S_L^{00} and 87% for C_L^{00} , as determined from a number of Monte Carlo experiments with event composition matched to the data). However, the two approaches differ in their sensitivity to the variations of the background composition, and have mostly uncorrelated systematic uncertainties associated with the B background PDFs and fit bias. Our two models represent the extreme approaches to describing the B backgrounds: one relies on the knowledge of the branching ratios associated with the dominant B backgrounds, and the other relies on the modeling of the kinematic distributions of B backgrounds in general. To further reduce these systematic effects, we average the results of the two models after the maximum likelihood fits.

Other four-pion final states, such as $B^0 \rightarrow \rho^0 \pi^+ \pi^-$ and $B^0 \rightarrow \pi^+ \pi^- \pi^+ \pi^-$, require special care. The rates for these modes are not well constrained [22], although their contributions are expected to be small in our invariant mass window. We parameterize the PDFs associated with these modes using the exclusive Monte Carlo samples, which assume uniform phase-space distributions of the final state mesons, and allow their yields to vary in the fit to the data. The absolute maximum of the likelihood occurs in the unphysical (negative) region for these yields, and we restrict the branching ratios for each of these modes to the range $[0..6] \times 10^{-6}$. The upper limit corresponds to several times the rate measured in Ref. [22]. With these restrictions, the yields for both $B^0 \rightarrow \rho^0 \pi^+ \pi^-$ and $B^0 \rightarrow \pi^+ \pi^- \pi^+ \pi^-$ decays converge identically to zero in the maximum likelihood fit, indicating no evidence for any contribution from these modes to the fit region.

5 RESULTS

We find excellent agreement between our two approaches to modeling B background events. Table 1 shows the average results, while the difference between the two models is used to determine the systematic uncertainty associated with B background description. The $B^0 \rightarrow \rho^0 \rho^0$ decay is observed with a significance of 3.6σ , as determined by the quantity $\sqrt{-2 \log(\mathcal{L}_0/\mathcal{L}_{\max})}$, where \mathcal{L}_{\max} is the maximum likelihood value, and \mathcal{L}_0 is the likelihood for a fit with the signal contribution set to zero. Both likelihoods include systematic uncertainties, which are assumed to be Gaussian-distributed. This significance level corresponds to a probability of background fluctuation to the observed signal yield of 2.8×10^{-4} . We do not observe significant event yields for $B^0 \rightarrow \rho^0 f_0(980)$ and $B^0 \rightarrow f_0(980) f_0(980)$ decays, nor of the non-resonant decays $B^0 \rightarrow \rho^0 \pi^+ \pi^-$ and $B^0 \rightarrow \pi^+ \pi^- \pi^+ \pi^-$. If the non-resonant contributions $B^0 \rightarrow \rho^0 \pi^+ \pi^-$ and $B^0 \rightarrow \pi^+ \pi^- \pi^+ \pi^-$ were ignored in the fit, the significance for $B^0 \rightarrow \rho^0 \rho^0$ signal would go up to 4.2σ . Background yields are found to be consistent with expectations. In Fig. 1 we show the projections of the fit results onto m_{ES} , ΔE , \mathcal{E} -shape, $m_{1,2}$, and $\cos \theta_{1,2}$ variables. Fig. 2 shows the distributions for the continuum $q\bar{q}$ component of the fit after subtracting the other components [23]. Fig. 3 shows the distribution of the likelihood ratio $L_{\text{sig}}/\sum_i \mathcal{L}_i$, where likelihoods \mathcal{L}_i include all signal and background PDFs. This ratio peaks near 1 for the signal events (Fig. 3b), and is highly peaked near zero for backgrounds.

We also fit the proper-time distribution of the data sample, and determine the CP -violating parameters S_L^{00} and C_L^{00} for the longitudinal component of the $B^0 \rightarrow \rho^0 \rho^0$ sample. The results are listed in Table 1. The projection plots of Δt distributions for \bar{B}^0 and B^0 tags, as well as the plot of the CP asymmetry, are shown in Fig. 4.

Table 1: Summary of results: event yields (n), corrected for fit bias; fraction of longitudinal polarization (f_L); selection efficiency (Eff) corresponding to measured polarization; branching fraction (\mathcal{B}_{sig}), and significance including systematic uncertainties. The systematic errors are quoted last. We also show the background event yields for $a_1\pi$, $q\bar{q}$, charmless, and other $B\bar{B}$ components (statistical uncertainties only).

Quantity	Value
$n(B^0 \rightarrow \rho^0 \rho^0)$	$85 \pm 28 \pm 17$
f_L	$0.70 \pm 0.14 \pm 0.05$
Eff (%)	23.8 ± 1.0
$\mathcal{B}_{\text{sig}} (\times 10^{-6})$	$0.84 \pm 0.29 \pm 0.17$
Significance, stat. only (σ)	4.0
Significance, syst. included (σ)	3.6
C_L^{00}	$0.4 \pm 0.9 \pm 0.2$
S_L^{00}	$0.5 \pm 0.9 \pm 0.2$
$n(B^0 \rightarrow \rho^0 f_0(980))$	-11 ± 16
$n(B^0 \rightarrow f_0(980)f_0(980))$	6 ± 6
$n(B^0 \rightarrow a_1^\pm \pi^\mp)$	296 ± 42
$n(\text{charmless})$	348 ± 64
$n(B\bar{B})$	2614 ± 134
$n(q\bar{q})$	62298 ± 268

6 SYSTEMATIC STUDIES

The systematic uncertainties for all physics parameters are summarized in Table 2. Dominant systematic uncertainties in the fit originate from statistical errors in the PDF parameterizations, due to the limited number of events in the control samples, variations in the B background branching ratios fixed in the fit, and from the potential fit bias. The PDF parameters are varied by their respective uncertainties to derive the corresponding systematic errors. The fit bias is studied in a large number of Monte Carlo experiments, in which signal and charmless B background events are fully simulated, and $b \rightarrow c$ background events and continuum $q\bar{q}$ events are sampled from their respective PDF. The uncertainty associated with the B background model is 4 events for the signal yield, 0.01 for f_L , 0.01 for C_L^{00} and 0.11 for S_L^{00} , derived from the difference between the fits for the two B background models. The systematic uncertainties due to the charmless background composition, arising from the uncertainties in the individual branching ratios and the CP content of B background [20, 24], are 5 events for the signal yield, 0.01 for f_L , 0.18 for C_L^{00} and 0.14 for S_L^{00} . The above systematic uncertainties do not scale with event yield and are included in the calculation of the significance of the result.

We estimate the systematic uncertainty due to the interference between the $B^0 \rightarrow \rho^0 \rho^0$ and $a_1^\pm \pi^\mp$ decays using simulated samples in which the decay amplitudes for $B^0 \rightarrow \rho^0 \rho^0$ are generated according to this measurement and those for $B^0 \rightarrow a_1^\pm \pi^\mp$ correspond to a branching fraction of $(33.2 \pm 4.8) \times 10^{-6}$ [25]. Their amplitudes are modeled with a Breit-Wigner function for all $\rho \rightarrow \pi\pi$ and $a_1 \rightarrow \rho\pi$ combinations and their relative phase is assumed to be constant across the phase space. The strong phases and CP content of the interfering state $a_1^\pm \pi^\mp$ are varied between zero and a maximum value using uniform prior distributions. We take the RMS variation of the average signal yield (14 events for the $\rho^0 \rho^0$ yield and 0.03 for f_L) as a systematic uncertainty.

Uncertainties in the reconstruction efficiency arise from track finding and particle identification, and are determined by dedicated studies on copious control data control samples. Uncertainties due to other selection requirements, such as vertex probability, track multiplicity, and thrust angle, amount to 2.4% for the event yields, and are negligible for the polarization and CP observables.

Table 2: *Summary of systematic uncertainties.*

Source	$n(B \rightarrow \rho^0 \rho^0)$ fraction	events	f_L	S_L^{00}	C_L^{00}
Multiplicative					
Number of B mesons	1.1%	–	–	–	–
Event selection	2.4%	–	–	–	–
PID selection	2.0%	–	–	–	–
Track finding	1.4%	–	–	–	–
MC statistics	<1%	–	< 0.01	< 0.01	< 0.01
$a_1\pi$ interference	–	14	0.025	0.07	0.07
Additive					
PDF variation	–	6	0.035	0.07	0.11
Fit bias	–	4	0.014	0.11	0.09
B background BR& CP	–	5	0.010	0.14	0.18
B background model	–	3	0.005	0.11	0.02
Total	3.6%	17	0.047	0.23	0.24

7 IMPLICATIONS FOR CKM ANGLE α

To constrain the penguin contributions to $B \rightarrow \rho\rho$ decays, we perform an isospin analysis, by minimizing a χ^2 term that includes the measured quantities expressed as the lengths of the sides of the isospin triangles. We use the measured branching fractions and fractions of longitudinal polarization of the $B^+ \rightarrow \rho^+ \rho^0$ [6] decays, the measured branching fractions, polarization, and CP parameters S_L^{+-} and C_L^{+-} determined from the time evolution of the longitudinally polarized $B^0 \rightarrow \rho^+ \rho^-$ decay [7], and finally the branching fraction, the polarization, and the CP parameters S_L^{00} and C_L^{00} of $B^0 \rightarrow \rho^0 \rho^0$ from this analysis. We assume uncertainties to be Gaussian and neglect $I = 1$ isospin contributions, electroweak loop amplitudes, non-resonant, and isospin-breaking effects.

Using the $B^0 \rightarrow \rho^0 \rho^0$ measurement we obtain a 68% (90%) CL limit on $|\alpha - \alpha_{\text{eff}}| < 14.5^\circ$ ($< 16.5^\circ$) where α_{eff} is constrained by the relation $\sin(2\alpha_{\text{eff}}) = S_L^{+-}/(1 - C_L^{+-2})^{1/2}$. Fig. 5 shows the confidence level with or without using the measured CP parameters S_L^{00} and C_L^{00} in the isospin

analysis fit. We observe the four solutions around zero as in the $B \rightarrow \pi\pi$ isospin analysis, but here, thanks to the additional constraint on S_L^{00} , one of the four solutions $\alpha - \alpha_{\text{eff}} = +11.3^\circ$ is favored.

8 CONCLUSION

In summary, we confirm our earlier evidence for $B^0 \rightarrow \rho^0\rho^0$ decays with a 3.6σ significance. We measure the $B^0 \rightarrow \rho^0\rho^0$ branching fraction of $(0.84 \pm 0.29 \pm 0.17) \times 10^{-6}$ and determine the longitudinal polarization fraction for these decays of $f_L = 0.70 \pm 0.14 \pm 0.05$. We also constrain the CP parameters C_L^{00} and S_L^{00} for the longitudinal part of the $B^0 \rightarrow \rho^0\rho^0$ final state:

$$\begin{aligned} S_L^{00} &= 0.5 \pm 0.9 \pm 0.2 \\ C_L^{00} &= 0.4 \pm 0.9 \pm 0.2 \end{aligned}$$

where the first uncertainty is statistical and the second is systematic. These measurements combined with those for $B^+ \rightarrow \rho^0\rho^+$ and $B^0 \rightarrow \rho^+\rho^-$ decays provide a constraint on the penguin uncertainty in the determination of the CKM unitarity angle α . We find no significant evidence for the decays $B^0 \rightarrow \rho^0 f_0$, $B^0 \rightarrow f_0 f_0$, $B^0 \rightarrow \rho^0\pi^+\pi^-$ and $B^0 \rightarrow \pi^+\pi^-\pi^+\pi^-$.

9 ACKNOWLEDGMENTS

We are grateful for the extraordinary contributions of our PEP-II colleagues in achieving the excellent luminosity and machine conditions that have made this work possible. The success of this project also relies critically on the expertise and dedication of the computing organizations that support *BABAR*. The collaborating institutions wish to thank SLAC for its support and the kind hospitality extended to them. This work is supported by the US Department of Energy and National Science Foundation, the Natural Sciences and Engineering Research Council (Canada), the Commissariat à l’Energie Atomique and Institut National de Physique Nucléaire et de Physique des Particules (France), the Bundesministerium für Bildung und Forschung and Deutsche Forschungsgemeinschaft (Germany), the Istituto Nazionale di Fisica Nucleare (Italy), the Foundation for Fundamental Research on Matter (The Netherlands), the Research Council of Norway, the Ministry of Science and Technology of the Russian Federation, Ministerio de Educación y Ciencia (Spain), and the Science and Technology Facilities Council (United Kingdom). Individuals have received support from the Marie-Curie IEF program (European Union) and the A. P. Sloan Foundation.

References

- [1] N. Cabibbo, Phys. Rev. Lett. **10**, 531 (1963); M. Kobayashi, T. Maskawa, Prog. Theor. Phys. **49**, 652 (1973).
- [2] M. Gronau, D. London, Phys. Rev. Lett. **65**, 3381 (1990).
- [3] Charge conjugate B decay modes are implied in this paper.
- [4] *BABAR* Collaboration, B. Aubert *et al.*, Phys. Rev. Lett. **91**, 171802 (2003); **94**, 131801 (2005); **98**, 111801 (2007).
- [5] Belle Collaboration, J. Zhang *et al.*, Phys. Rev. Lett. **91**, 221801 (2003).

- [6] *BABAR* Collaboration, B. Aubert *et al.*, Phys. Rev. Lett. **97**, 261801 (2006).
- [7] *BABAR* Collaboration, B. Aubert *et al.*, Phys. Rev. D **69**, 031102 (2004); Phys. Rev. Lett. **93**, 231801 (2004); arXiv:0705.2157 [hep-ex], to appear in Phys. Rev. D.
- [8] Belle Collaboration, A. Somov *et al.*, Phys. Rev. Lett. **96**, 171801 (2006); arXiv:hep-ex/0702009, submitted to Phys. Rev. D.
- [9] A. Ali *et al.*, Z. Phys. C **1**, 269 (1979).
- [10] *BABAR* Collaboration, B. Aubert *et al.*, Phys. Rev. Lett. **91**, 171802 (2003); Belle Collaboration, K.-F. Chen *et al.*, Phys. Rev. Lett. **91**, 201801 (2003).
- [11] A. Datta *et al.*, arXiv:0705.3915 [hep-ph], to appear in Phys. Rev. D.
- [12] A.F. Falk *et al.*, Phys. Rev. D **69**, 011502 (2004).
- [13] *BABAR* Collaboration, B. Aubert *et al.*, Nucl. Instrum. Methods Phys. Res., Sect. A **479**, 1 (2002).
- [14] PEP-II Conceptual Design Report, SLAC-R-418 (1993).
- [15] *BABAR* Collaboration, B. Aubert *et al.*, Phys. Rev. D **70**, 032006 (2004).
- [16] The *BABAR* detector Monte Carlo simulation is based on GEANT4: S. Agostinelli *et al.*, Nucl. Instrum. Methods Phys. Res., Sect. A **506**, 250 (2003).
- [17] *BABAR* Collaboration, B. Aubert *et al.*, Phys. Rev. D **66**, 032003 (2002); Phys. Rev. Lett. **94**, 161803 (2005).
- [18] E791 Collaboration, E. M. Aitala *et al.*, Phys. Rev. Lett. **86**, 765 (2001).
- [19] Particle Data Group, W.-M. Yao *et al.*, J. Phys. G33, 1 (2006).
- [20] The Heavy Flavor Averaging Group, E. Barberio *et al.*, arXiv:0704.3575 [hep-ex] and online update at <http://www.slac.stanford.edu/xorg/hfag>
- [21] *BABAR* Collaboration, B. Aubert *et al.*, preprint *BABAR-PUB-07/034*, submitted to Phys. Rev. Lett.
- [22] Belle Collaboration, K. Abe *et al.*, preprint arXiv:0706.3279 [hep-ex] (2007).
- [23] M. Pivk and F. R. Le Diberder, Nucl. Instrum. Methods Phys. Res., Sect. A **555**, 356 (2005).
- [24] *BABAR* Collaboration, B. Aubert *et al.*, Phys. Rev. Lett. **98**, 181803 (2007).
- [25] *BABAR* Collaboration, B. Aubert *et al.*, Phys. Rev. Lett. **97**, 051802 (2006).

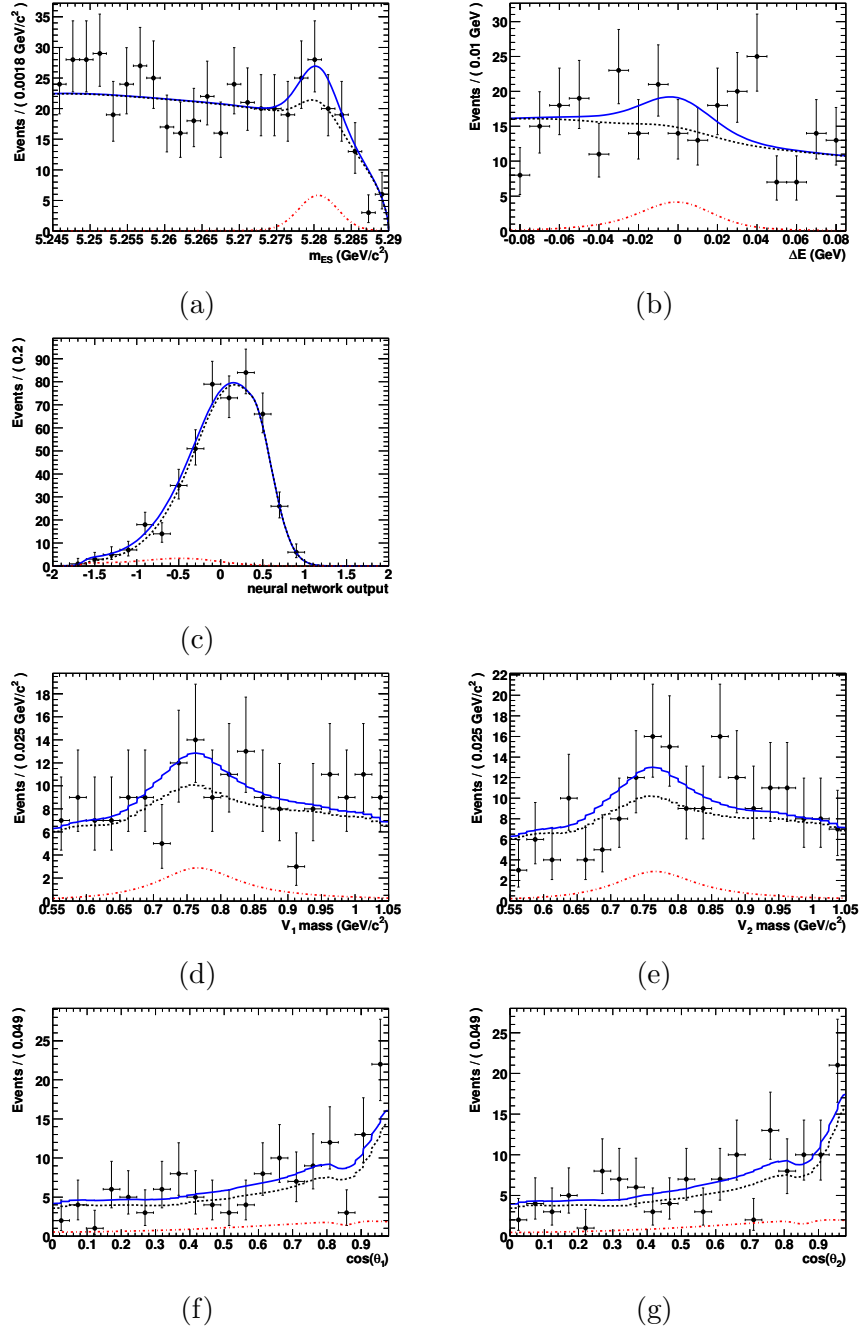


Figure 1: Projections of the multidimensional fit onto (a) m_{ES} , (b) ΔE , (c) event shape variable \mathcal{E} , (d,e) di-pion invariant masses m_1 and m_2 , and (f,g) cosines of the helicity angles $\cos\theta_{1,2}$, after a requirement on the signal-to-background probability ratio with the plotted variable excluded. This requirement enhances the fraction of signal events in the sample while keeping approximately 25% of signal events. The data points are overlaid by the solid blue line, which corresponds to the full PDF projection. The individual $B^0 \rightarrow \rho^0 \rho^0$ PDF component is also shown with a dot-dashed red line. The sum of all other PDFs (including $B^0 \rightarrow \rho^0 f_0$ and $B^0 \rightarrow f_0 f_0$ components) is shown as the dashed black line. The D -meson veto causes the acceptance dip seen in (f,g).

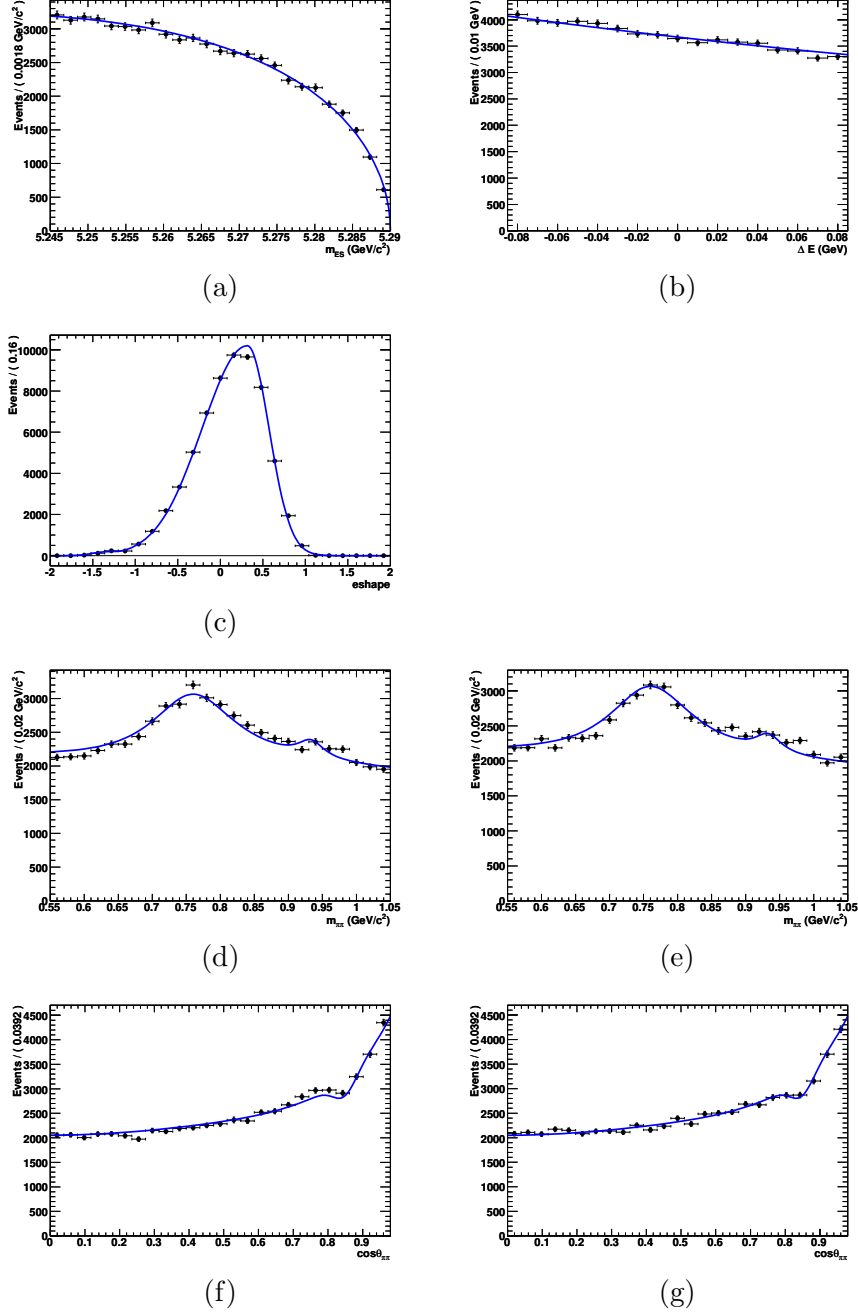


Figure 2: Signal-subtracted projections (sPlots) of the multidimensional fit onto (a) m_{ES} , (b) ΔE , (c) event shape variable \mathcal{E} , (d,e) di-pion invariant masses m_1 and m_2 , and (f,g) cosines of the helicity angles $\cos\theta_{1,2}$. The data are weighed to enhance the continuum $q\bar{q}$ events and effectively subtract all other fit components. The data points are overlaid by the solid blue line, which corresponds to the $q\bar{q}$ PDF component.

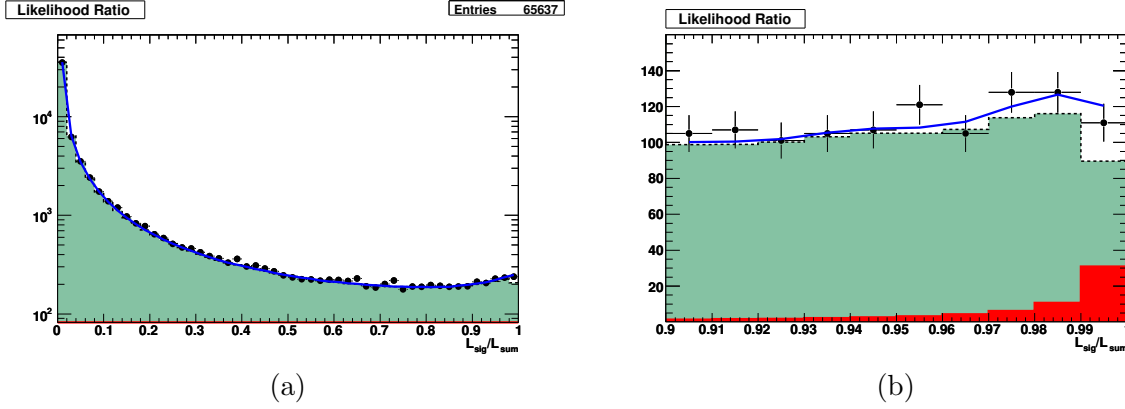


Figure 3: Likelihood ratio $\mathcal{L}_{\text{sig}}/\sum_i \mathcal{L}_i$, where likelihoods \mathcal{L}_i include all signal and background PDFs. Data points are overlaid by a blue curve, which corresponds to the full PDF. The shaded teal histogram and the black dashed line correspond to the sum of background PDFs, and the red histogram corresponds to the signal contribution. Full range (a) and a zoom-in into the signal region (b) are shown.

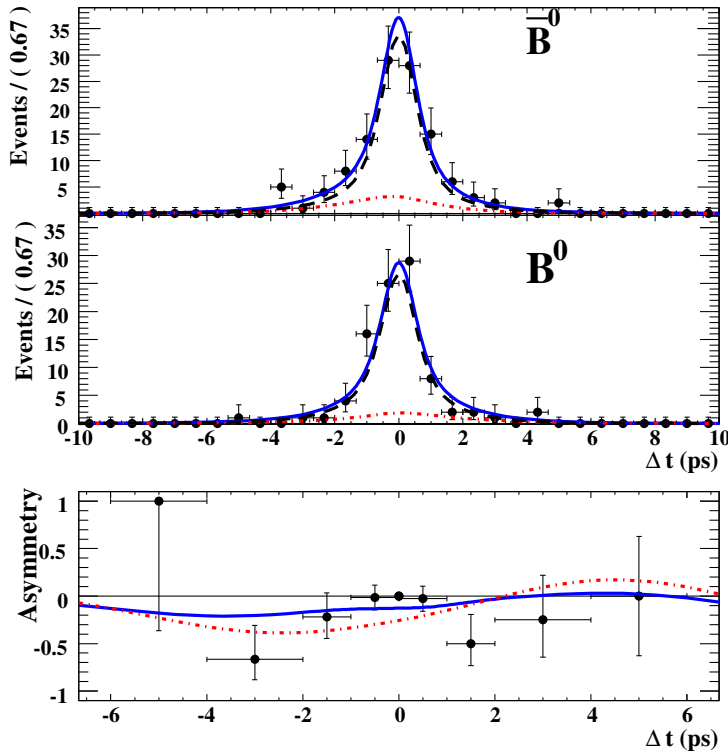


Figure 4: Projections of the multidimensional fit onto Δt variable for (top) \bar{B}^0 tags and (middle) B^0 tags. CP asymmetry \mathcal{A}_{CP} is shown in the bottom plot. The solid blue line represents the projection of the total PDF, the red dot-dashed line is the $B^0 \rightarrow \rho^0 \rho^0$ contribution, and the dashed black line corresponds to the sum of all backgrounds. A likelihood cut $\mathcal{L}_{\text{sig}}/\sum_i \mathcal{L}_i > 0.99$ is applied to enhance the signal contribution.

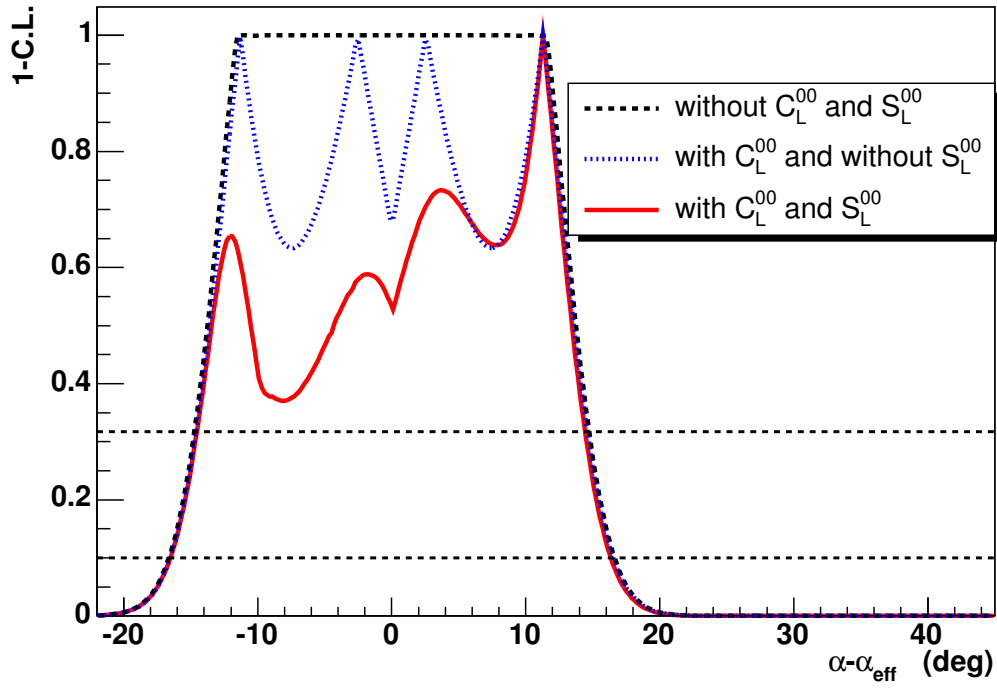


Figure 5: Confidence level on $\alpha - \alpha_{\text{eff}}$ obtained from the isospin analysis discussed in the text. The solid line CL includes the CP parameters C_L^{00} and S_L^{00} in the fit. The dotted line corresponds to the usual isospin analysis without S_L^{00} . The dashed curve is obtained without the two CP parameters S_L^{00} and C_L^{00} . The horizontal dashed lines correspond to the 68% (top) and 90% (bottom) CL intervals.